A Charge Equalizer With a Combination of APWM and PFM Control Based on a Modified Half-Bridge Converter

Chihchiang Hua, *Member, IEEE*, and Yi-Hsiung Fang

***Abstract*—A charge equalizer with a combination of asymmetrical pulse width modulation and pulse frequency modulation control based on a modified half-bridge converter for electric vehicles is proposed in this paper. The reliability of the charge equalizer can be improved because the split capacitors are not required and the soft switching of power switches can be achieved by the proposed control. In addition, with the proposed rectification, the number of bridge rectifiers at the secondary side of the transformer can be reduced by half, which also cuts the cost and conduction loss by half. The circuit topology, operation analysis, and control strategy of the proposed charge equalizer are described in detail. Finally, the experimental results are provided to verify the feasibility and performance of the proposed charge equalizer.**

***Index Terms*—Cell balancing, charge equalizer, series-connected batteries.**

I. Introduction

SOME lithium-ion (Li-ion) batteries with different cathode materials, such as $LiCoO_2$, $LiNiO_2$, or $LiFePO_4$, are widely used for the energy-storage systems, uninterruptible power supplie, and electric vehicles (EVs) [1]–[14]. The Li-ion batteries not only have the features of high energy density, high power density, and high conversion efficiency, but also have the merits of low self-discharge rate, high-current discharge, and no memory effect [1]–[12], [15]. Moreover, the high-voltage sources can be achieved by connecting fewer Li-ion batteries than other popular batteries since the nominal-cell voltages of a Li-ion battery, a lead-acid battery, and a Ni-MH battery are 3.3–3.7, 2, and 1.2 V, respectively [1], [2], [15]–[17].

In the EV's applications, the electric motor requires high voltages, which may not be provided by one battery cell. Therefore, several batteries (typically over 100 cells) have to be connected in series to obtain the required high voltage (typically over 300 V) of an electric motor. However, the overcharging or overdischarging phenomenon may occur when the batteries are charged (discharged) in series due to their differences in self-discharge rate and internal impedance when they were manufactured [1]–[10], [13], [16]–[25]. For the Li-ion battery cell, the voltage limits for the charging and discharging are 3.6–4.2 and 2.2–2.5 V, respectively. The Li-ion battery will become combustible if it is overcharged, and short-circuit conditions or even explosion may occur when it is overdischarged since the metallic copper is generated inside the battery [1]–[8], [11]–[13], [15], [16], [18]–[23], [26].

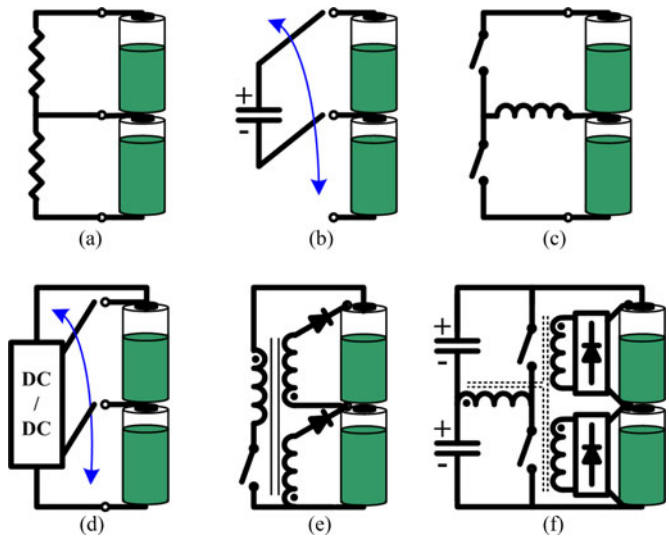

Fig. 1. Common charge equalizers. (a) Shunting resistor type. (b) Switched capacitor type. (c) Buck–boost converter type. (d) Selective isolated converter type. (e) Multiwinding transformer type (fly-back converter). (f) Multiwinding transformer type (Half-bridge converter).

Although the nominal voltage of $LiFePO_4$ battery is slightly lower than that of the other Li-ion batteries, it still has the advantages of large discharging current (continuous discharge at 10 C), high-cycle life (more than 2000 times), and very low self-discharge rate (less than 8% per month). Moreover, it is not easy to explode because the olivine-type structure of $LiFePO_4$ battery is stable. Hence, the $LiFePO_4$ battery is suitable for the EV's applications that need high safety. To avoid overcharging or overdischarging phenomenon's, the charging equalization control for Li-ion batteries needs to be implemented for the battery system [2]–[7], [9], [10], [12]–[14], [16], [18], [19], [23], [26]–[29].

The shunting resistor equalizer is the simplest charge equalization, yet it is not an efficient method since the energy of a battery is dissipated to the shunting resistors as shown in Fig. 1(a). In order to reduce the continuous energy loss, the shunting resistors can be replaced by Zener diodes or connected

Manuscript received November 28, 2014; revised April 17, 2015 and February 10, 2015; accepted July 2, 2015. Date of publication July 16, 2015; date of current version November 30, 2015. Recommended for publication by Associate Editor L. Chang.

C. Hua is with the Department of Electrical Engineering, National Yunlin University of Science and Technology, Douliou 640, Taiwan. (e-mail: huacc@yuntech.edu.tw).

Y.-H. Fang is with the Graduate School of Engineering Science and Technology, National Yunlin University of Science and Technology, Douliou 640, Taiwan (e-mail: d10210009@yuntech.edu.tw).

Color versions of one or more of the figures in this paper are available online at http://ieeexplore.ieee.org.

Digital Object Identifier 10.1109/TPEL.2015.2453438

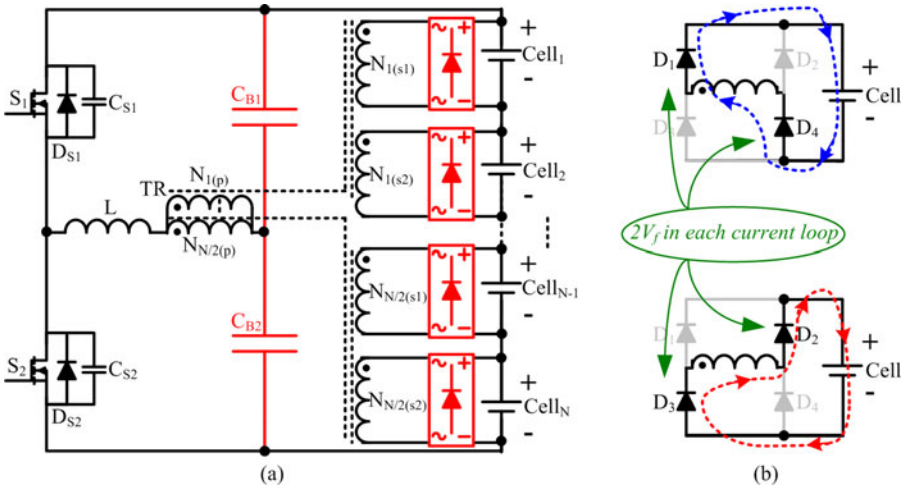

Fig. 2. (a) General charge equalizer with a half-bridge converter. (b) Current loops of a bridge rectifier.

with active switches. From the above discussions, the dissipative equalizers are not suitable for a large-scale battery pack. Thus, the nondissipative equalizers based on an energy transfer concept were developed [2]–[6], [17]–[21], [23], [24], [27].

The switched-capacitor equalizer is simple and no voltage sensors are required as shown in Fig. 1(b). This method is based on two voltage sources (battery and capacitor) connected in parallel, which results in a large inrush current due to a large voltage difference between battery and capacitor [2]–[5], [16]–[18], [20]–[22], [24], [25].

The buck–boost converter-type equalizer can efficiently distribute the energy among the batteries because it can deliver the energy from a low-voltage battery to a high-voltage battery as shown in Fig. 1(c). However, it needs an accurate control, more sensors and switches [2], [4], [8], [10], [13], [16]–[18], [20], [21], [23], [25]–[27].

The selective isolated converter-type equalizer as shown in Fig. 1(d) used only one converter to reduce the handmade components, such as the inductor and the transformer. However, its cannot provide energy to more than one battery at the same time. In addition, the cost is high if the system uses electrical relays as the selective switches [5], [6], [8], [17], [20].

The multiwinding transformer-type equalizer is based on the same emf induced in different windings as shown in Fig. 1(e) and (f). Although it uses only one magnetic core and fewer active switches, the implementation is complicated with a lot of batteries in the pack. Hence, the multiwinding transformer type can be replaced by multiple transformers type for simple modularization [2], [4], [5], [7], [16]–[21], [25]–[27].

From the above discussions, the nondissipative equalizers are well suited for the applications of EV's batteries. Furthermore, a good charge equalizer should have features of an easy control, fewer active power switches, good reliability, high conversion efficiency, and high power density. In this paper, a novel charge equalizer is presented for the battery system of EV. The circuit topology, operation analysis, and control strategy of the proposed charge equalizer are described in detail. Finally, a prototype circuit is implemented to confirm the feasibility and performance of the proposed charge equalizer.

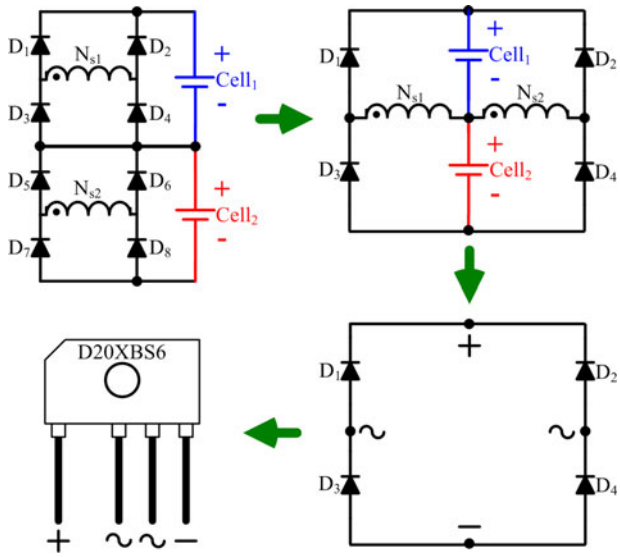

Fig. 3. Evolution of the proposed rectification.

II. Circuit Topology of the Proposed Charge Equalizer

In order to improve the reliability of the battery system, the charge equalizer with fewer active components is preferred. Fig. 2(a) shows the general charge equalizer based on a half-bridge converter with only two power switches. However, the lifetime of the charge equalizer may be reduced because the conventional half-bridge converter needs two split electrolytic capacitors that have shorter lifetime than the other components in the circuit. Moreover, the bridge rectifiers are not suitable for battery applications because of the low battery cell voltage and the double voltage drops in the current loop as shown in Fig. 2(b).

A new rectification is proposed as shown in Fig. 3. Therefore, the number of the bridge rectifiers can be reduced by half and there is only one voltage drop in the current loop. In short, the cost and the conduction loss of the rectifier can be reduced.

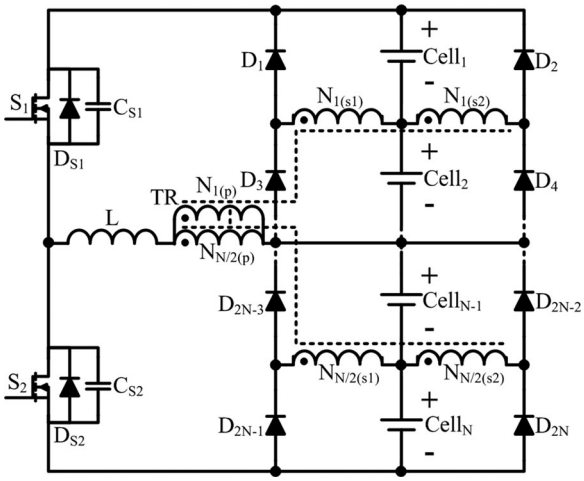

Fig. 4. Proposed charge equalizer.

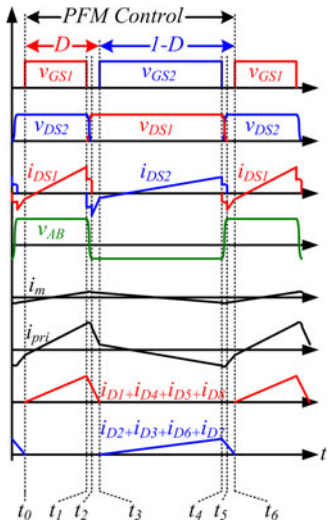

Fig. 5. Key waveforms.

The proposed charge equalizer is shown in Fig. 4. A modified half-bridge converter without any split electrolytic capacitor is applied at the primary side of the transformer, and the proposed rectification is applied at the secondary side. There are *N* cells in a battery module, and the number of transformers is *N/2*.

Furthermore, the power switches with soft switching are used to increase the circuit efficiency if the transformer operates in the first and third quadrants of the *B–H* loop, and the power switches are driven by using the asymmetrical pulse width modulation (APWM) control.

III. Operation Analysis

The operation of the proposed charge equalizer consists of six modes as shown in Fig. 5. Before the analysis, several assumptions are made as follows:

1) there are four batteries in a module and the battery voltage is constant;
2) S_1 and S_2 are the MOSFETs, D_{S1} and D_{S2} are the body diodes of MOSFETs, C_{S1} and C_{S2} are the parasitic capacitances of MOSFETs and they are identical;
3) L_m and L are the magnetic inductances for the transformer and choke inductances, respectively;
4) $D_1 - D_8$ are the rectifier diodes;
5) magnetic inductance L_m is relative large, thus magnetic current i_m can be neglected.

Mode 1 (t_0–t_1): The equivalent circuit of mode 1 is shown in Fig. 6(a). Assuming N_{1p}: N_{2p}: N_{1s1}: N_{1s2}: N_{2s1}: $N_{2s2} = n : n : 1 : 1 : 1 : 1$, thus $v_{1p} = v_{2p} = v_P, v_{1s1} = v_{1s2} = v_{2s1} = v_{2s2} = v_S$. In addition, the cell$_1$ is assumed to be the worst battery and the voltage of cell$_1$ is V_{cell1}. S_1 is turned ON in this mode; thus, the energy of cell$_1$ and cell$_2$ can be transferred to the secondary side of the transformer.

From Fig. 6(a), the following equation is obtained:

$$i_{\text{pri}}(t_1) = i_{\text{pri}}(t_0) + \left(\frac{V_H - n(V_{\text{cell1}} + V_f)}{L}\right)(t_1 - t_0) \quad (1)$$

where V_f is the forward-bias voltage drop of the diode in the bridge rectifier.

Mode 2 (t_1–t_2): The circuit state of mode 2 is shown in Fig. 6(b). The parasitic capacitance C_{S1} is charged and the C_{S2} is discharged because the current of inductance *L* is still flowing when S_1 is turned OFF in this mode.

Parasitic capacitances C_{S1} and C_{S2} share the current of inductance *L*. (The values of C_{S1} and C_{S2} can be obtained by referring the relationship between capacitance and V_{DS} in datasheet of MOSFET). In order to achieve ZVS turn ON of a power switch S_2, the ZVS conditions are given as follows:

Condition 1

$$\frac{1}{2}Li_{\text{pri}}^2(t_1) \geq \frac{1}{2}(C_{s1} + C_{s2})(V_H + V_L)^2. \quad (2)$$

Condition 2

$$\frac{(V_H + V_L)}{i_{\text{pri}}(t_1)} \times (C_{s1} + C_{s2}) \leq T_d \quad (3)$$

where T_d is the deadtime. In the resonant region $(t_1 - t_2)$

$$i_{\text{pri}}(t_2) \cong i_{\text{pri}}(t_1). \quad (4)$$

Mode 3 (t_2–t_3): The circuit state of mode 3 is shown in Fig. 6(c). In this mode, C_{S1} is charged to $V_H + V_L$, and C_{S2} is discharged to 0 V. The current of inductance *L* is still flowing through the body diode D_{S2}, and S_2 has to be turned ON in this mode to achieve soft switching. Otherwise, $V_{S1} = V_H$ and $V_{S2} = V_L$, then the condition of soft switching for S_2 will be lost.

$i_{\text{pri}}(t_3)$ is expressed as follows:

$$i_{\text{pri}}(t_3) = i_{\text{pri}}(t_2) - \left(\frac{V_L + n(V_{\text{cell1}} + V_f)}{L}\right)(t_3 - t_2). \quad (5)$$

Mode 4 (t_3–t_4): S_2 is turned ON in this mode thus the energy of cell$_3$ and cell$_4$ can be transferred to the secondary side of the transformer. From Fig. 6(d), the following equation is obtained:

$$i_{\text{pri}}(t_4) = i_{\text{pri}}(t_3) - \left(\frac{V_L - n(V_{\text{cell1}} + V_f)}{L}\right)(t_4 - t_3). \quad (6)$$

Mode 5 (t_4–t_5): The circuit state of mode 5 is shown in Fig. 6(e). The parasitic capacitances C_{S2} is charged and C_{S1} is discharged because the current of inductance *L* is still flowing when S_2 is turned OFF in this mode.

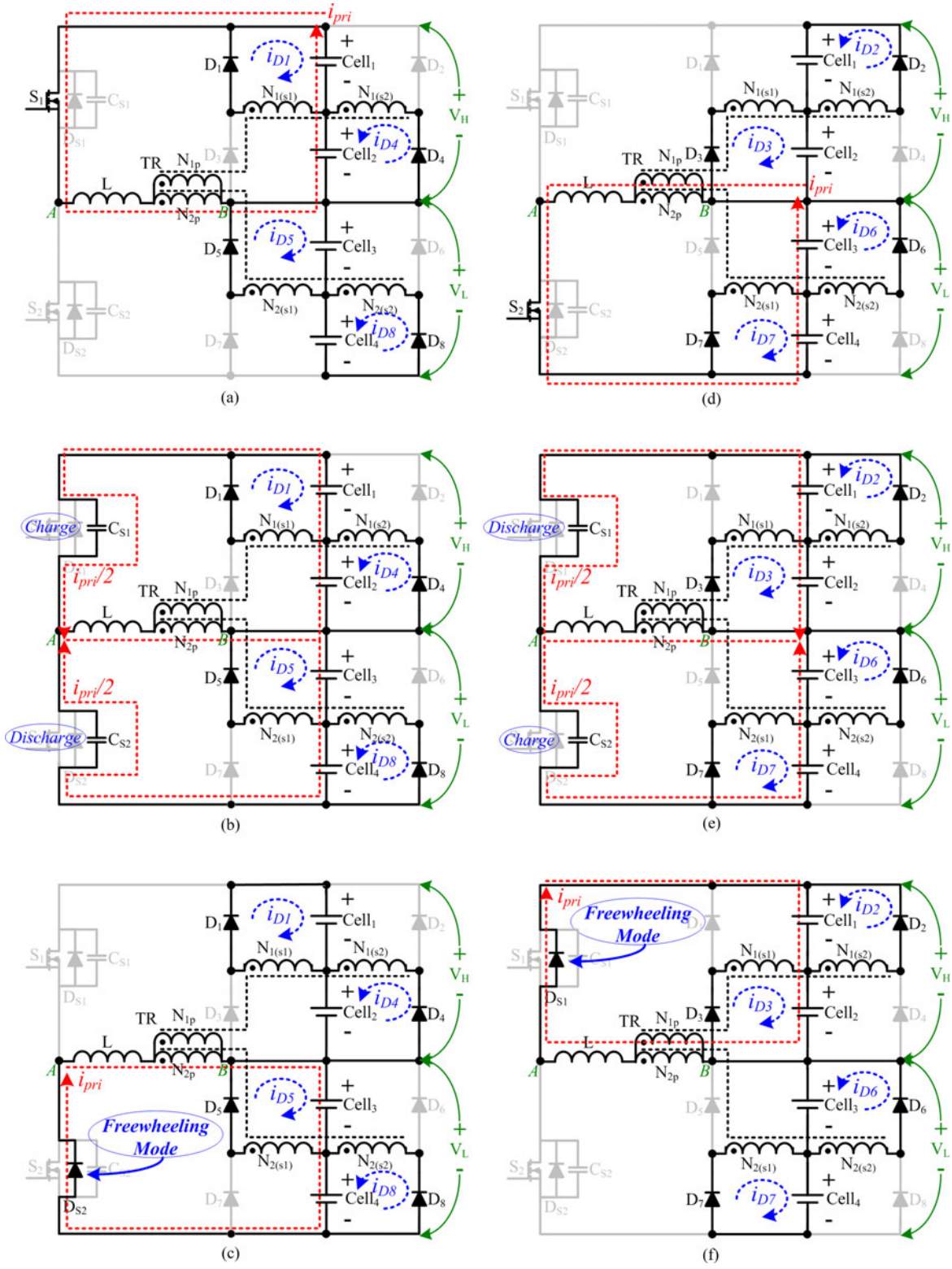

Fig. 6. Circuit state. (a) Mode 1. (b) Mode 2. (c) Mode 3. (d) Mode 4. (e) Mode 5. (f) Mode 6.

The parasitic capacitances C_{S1} and C_{S2} share the current of inductance L. To achieve ZVS turn ON of power switch S_2, the ZVS conditions are given as follows:

Condition 1

$$\frac{1}{2}Li_{\mathrm{pri}}^2(t_4) \geq \frac{1}{2}(C_{s1}+C_{s2})(V_H+V_L)^2. \tag{7}$$

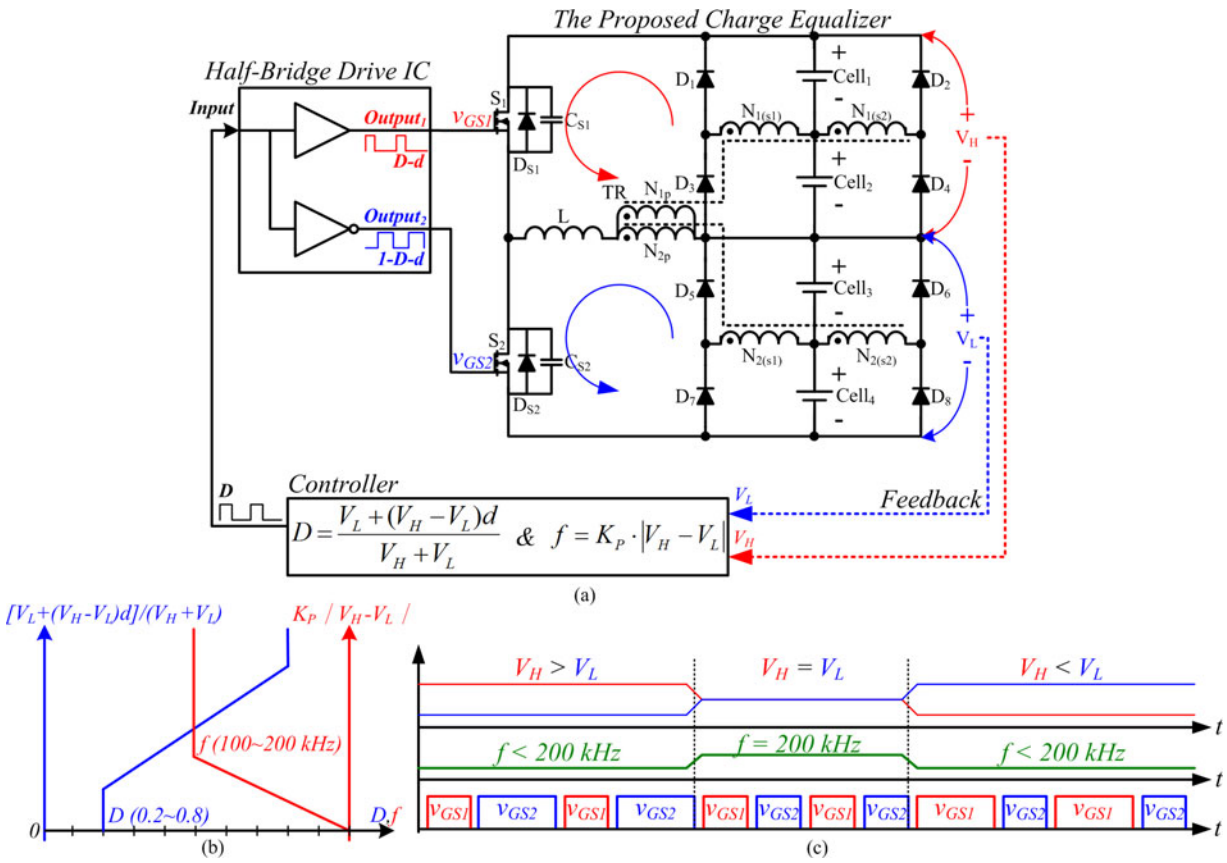

Fig. 7. (a) Proposed circuit with feedback diagram. (b) Ranges for duty ratio D and frequency f. (c) Drive signals of switches v_{GS1} and v_{GS2} with respect to V_H and V_L.

Condition 2

$$\frac{(V_H + V_L)}{-i_{\rm pri}(t_4)} \times (C_{s1} + C_{s2}) \le T_{\rm d} \tag{8}$$

where T_d is the deadtime. In the resonant region $(t_4 - t_5)$

$$i_{\rm pri}(t_5) \cong i_{\rm pri}(t_4). \tag{9}$$

Mode 6 (t_5–t_6): The circuit state of mode 6 is shown in Fig. 6(f). In this mode, the C_{S2} is charged to $V_H + V_L$, and C_{S1} is discharged to 0 V. The current of inductance L is still flowing through the body diode D_{S1}, and S_1 has to be turned ON in this mode to achieve soft switching. Otherwise, $V_{S1} = V_H$ and $V_{S2} = V_L$, then the condition of soft switching for S_1 will be lost. $i_{\rm pri}(t_6)$ is expressed as follows:

$$i_{\rm pri}(t_6) = i_{\rm pri}(t_5) + \left(\frac{V_H + n(V_{\rm cell1} + V_f)}{L}\right)(t_6 - t_5). \tag{10}$$

IV. Control Strategy

According to the voltage–second principle of the transformer core, the following equation is obtained:

$$V_H \times (DT - T_d) = V_L \times [(1 - D)T - T_d] \tag{11}$$

where T and T_d are the period and the deadtime of power switches, respectively. Assuming d is T_d/T. Therefore, the duty ratios of v_{GS1} and v_{GS2} are $D - d$ and $1 - D - d$, respectively, and the duty ratio of the v_{GS1} can be expressed as

$$D - d = \frac{V_L(1 - 2d)}{V_H + V_L}. \tag{12}$$

In addition, because the half-bridge drive IC can easily drive the floating power switches, it is very suitable for the half-bridge converter, synchronous buck converter, and active-clamp forward converter, etc. Hence, a half-bridge drive IC is used in the proposed charge equalizer with a modified half-bridge converter, and the proposed circuit with feedback diagram is shown in Fig. 7(a). Assuming the duty ratio of input signal of the half-bridge drive IC is D, the duty ratios of the output signals are $D - d$ and $1 - D - d$, and the following equation is obtained:

$$D = \frac{V_L + (V_H - V_L)d}{V_H + V_L}. \tag{13}$$

On the other hand, the charge equalization for batteries can be flexibly controlled by the pulse frequency modulation (PFM) control, and the following equation is obtained:

$$f = 200 - K_P \cdot |V_H - V_L| \tag{14}$$

where f (kHz) is the switching frequency of power switches, and K_P is the proportional coefficient of the PFM control. If the V_H equals V_L, the switching frequency of power switches is set to 200 kHz to reduce the circulating current. Otherwise, the

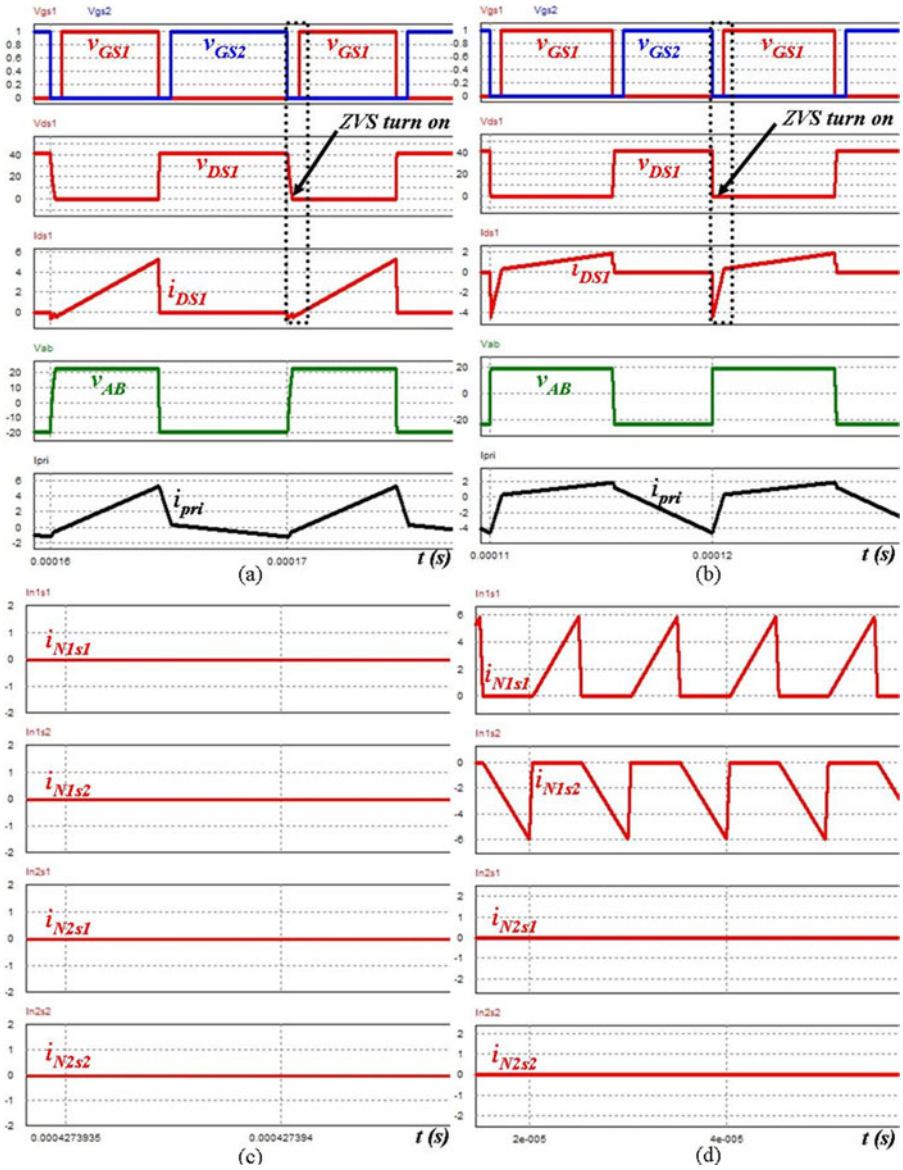

Fig. 8. Simulated results. (a) Waveforms of the primary side ($V_{\rm H} > V_{\rm L}$). (b) Waveforms of the primary side ($V_{\rm H} < V_{\rm L}$). (c) Waveforms of the secondary side ($V_{\rm Cell1} = V_{\rm Cell2} = V_{\rm Cell3} = V_{\rm Cell4}$). (d) Waveforms of the secondary side ($V_{\rm Cell1}$ is the worst battery).

frequency will be reduced progressively to increase the charge equalization current when the difference between V_H and V_L increases.

Finally, the schematic diagram of ranges for duty ratio D and frequency f is shown in Fig. 7(b), and the timing diagram that corresponds to V_H and V_L is shown in Fig. 7(c).

In order to preliminarily confirm the feasibility of the proposed equalizer, a Powersim simulation software is used. Fig. 8 shows the simulation results, which agree with the previous operation analysis and the waveforms of Fig. 5. At the primary side of a transformer, the APWM technique is used to avoid the saturation of transformer core and the power switch is turned ON with ZVS to eliminate the switching loss as shown in Fig. 8(a) and (b). According to the Faraday's law, the same voltages are induced on all windings with the same number of turns at the secondary side of the transformer. From the waveforms of Fig. 8(c), no current flows into the batteries since all batteries have the same voltage. In addition, the charge equalization can be achieved because the low-voltage battery absorbs higher current than the high-voltage battery as shown in Fig. 8(d). Based on the simulations and previous discussions, the proposed system is designed and constructed. The circuit parameters and the experimental results will be given in the next section.

V. Experimental Results

To investigate the performance of the proposed charge equalizer, the experimental prototype is constructed. Fig. 9 shows the test configuration and the test bench for the proposed system. The laboratory environment temperature is approximately 25 °C. The battery module voltages are recorded with a data recorder YOKOGAWA MX100, and the digital oscilloscope is

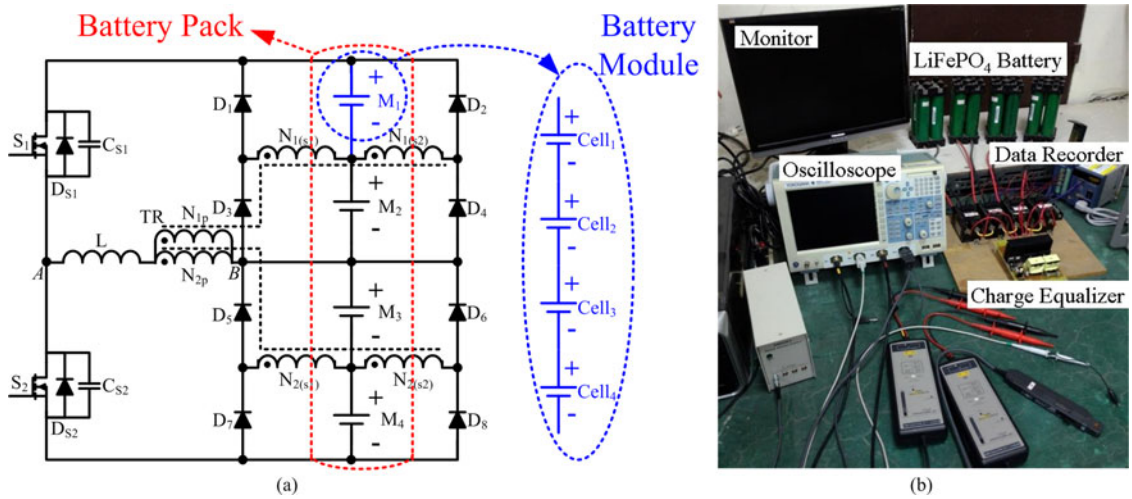

Fig. 9. (a) Test configuration and (b) the test bench for the proposed charge equalizer.

TABLE I
SPECIFICATIONS OF BATTERY AND PROPOSED EQUALIZER

Battery	Battery type	$LiFePO_4$
	Nominal voltage	3.2 V/cell
	Nominal capacity	12 Ah
	Charge limit voltage	3.65 V/cell
	Discharge cut-off voltage	2.1 V/cell
Proposed circuit	Power switch	IRFB4410Z
	Schottky bridge rectifier	D20XBS6
	Size of core	PQ3230
	Inductor	2 μH
	Turns ratio of transformer	$n = 2$
Half-bridge drive IC	Part name	L6384
	Deadtime T_d	0.5 μs
	Input signal D	0.2–0.8
	Frequency f	100–200 kHz

YOKOGAWA DL9040. There are four battery cells in a battery module, and a battery pack is consists of four battery modules connected in series. The specifications of the battery and the proposed charge equalizer are listed in Table I. When the reasonable inductance is selected, the maximum output current of the proposed charge equalizer can be enhanced to shorten the equalization time by selecting a lower minimum operation frequency, but the size of a transformer core has to increase to avoid the saturation of a transformer core. On the other hand, when all of the battery voltages are getting close, the output current can be reduced by increasing the maximum operation frequency. However, the operation frequency range should be designed to provide a good dynamic performance. Therefore, the reasonable operation frequency range is 100–200 kHz and the duty ratio range is 0.2–0.8. To reduce the circulating current, which results in conduction loss in the current loop, from the primary to secondary side of the transformer when all battery voltages are the same, the following equation is obtained for the system with transformer turns ratio *n*:

$$n = \frac{\text{The number of batteries}}{2}. \tag{15}$$

For example, the *n* will be set as 2 if the number of batteries is 4. If $n < 2$, a circulating current flows from the primary to secondary side of the transformer when the voltages of all batteries are the same. Otherwise, if $n > 2$, the charge equalization performance may be poor because the emf at the secondary side of the transformer is lower than the case of $n < 2$. On the other hand, the maximum flux density of the transformer core has to be considered based on Faraday's law for the system transformer design. Hence, the number of transformer primary winding is chosen as 6 to avoid the core saturation, and the turns ratio of 2 is used for the system transformer.

In order to simplify the layout of a printed circuit board (PCB), D_1–D_4 and D_5–D_8 can be replaced by two bridge rectifiers.

A. Proposed Charge Equalizer Test

Based on the voltage–second principle of the transformer core, the APWM technique is applied in the proposed charge equalizer as shown in Fig. 10. Fig. 10(a) and (c) shows that the switching frequency decreases hence the difference between V_H and V_L increases, and the maximum switching frequency 200 kHz appears when V_H is equal to V_L, as shown in Fig. 10(b).

The v_{DS1} is reduced to zero before v_{GS1} becomes high level. Therefore, the power switch S_1 can be turned ON with ZVS to reduce the switching loss as shown in Fig. 11.

The Faraday's law is applied to the secondary side of the proposed charge equalizer, and assume $i_{N1s1} = i_{D1} + (-i_{D3})$, $i_{N1s2} = i_{D2} + (-i_{D4})$, $i_{N2s1} = i_{D5} + (-i_{D7})$, $i_{N2s2} = i_{D6} + (-i_{D8})$. Fig. 12(a) shows that no currents flow into the battery modules because their voltages are the same. On the contrary, the charge equalization currents only flow into the battery module M_1 because its voltage is the lowest in the battery pack as shown in Fig. 12(b).

B. Charge Equalization Performance Test

The charge equalization result for the system with battery pack is shown in Fig. 13, the initial voltages of the battery modules (M_1–M_4) are 11.60, 12.83, 13.15, and 13.54 V, respectively,

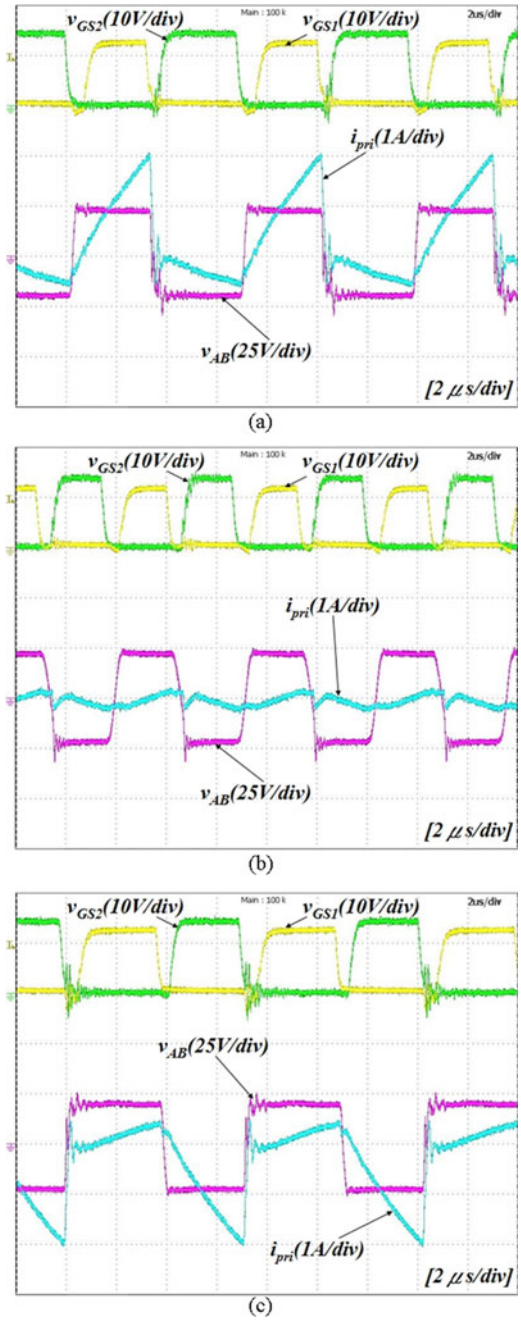

Fig. 10. Measured waveforms of v_{GS1}, v_{GS2}, v_{AB}, and $i_{\rm pri}$. (a) $V_H > V_L$. (b) $V_H = V_L$. (c) $V_H < V_L$.

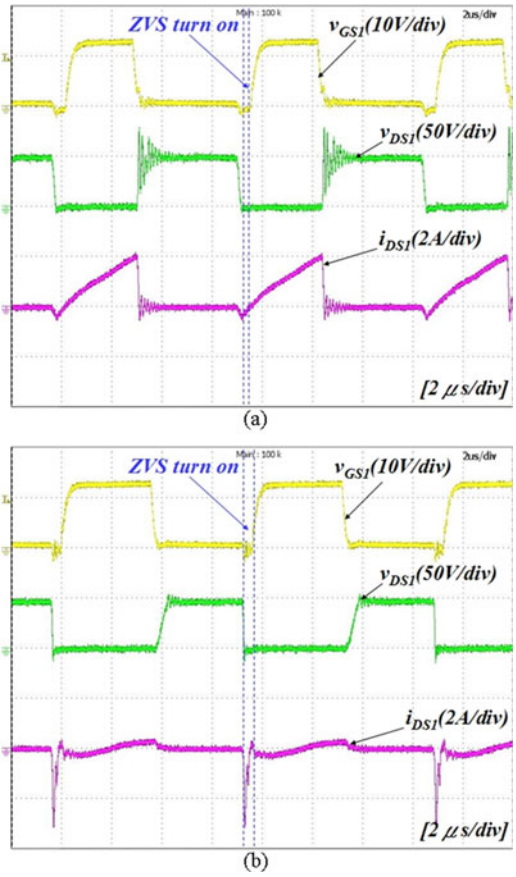

Fig. 11. Measured waveforms for S_1 with ZVS turn ON. (a) $V_H > V_L$. (b) $V_H < V_L$.

and the initial maximum voltage difference is 1.94 V. After the equalization, the steady battery module voltages are 12.89, 12.92, 13.13, and 13.28 V, respectively, and the maximum voltage difference is 0.39 V. Moreover, the circulating current from the primary side to the secondary side of the transformer is reduced. Due to the voltage drops of power device, the nonzero maximum voltage difference will always exists.

The estimated efficiencies of the proposed equalizer (refer to Fig. 4) are compared with those of the general equalizer [refer to Fig. 2(a)] as shown in Fig. 14(a). The power losses from the MOSFET switches and copper wire increase when the temperature increases, but the power losses from the Schottky bridge rectifiers and the transformer core decrease. Therefore, the temperature is neglected for the efficiency analysis since the temperature variations have a little effect on the power loss. As shown in Fig. 14(a), the estimated efficiencies of the proposed equalizer are about 6% greater than those of the general equalizer. In the applications of low output voltage, the conduction loss of secondary-side diodes dominates the power loss for the system. Although the synchronous rectification can be used to reduce the conduction loss, the control is complicated and the reliability decreases with the number of cells in a battery system. For the proposed equalizer, a Schottky bridge rectifier with a new rectification is designed for reducing the conduction loss since there is only one voltage drop in the current loop. In addition, the proposed circuit is easily expanded for the applications that require a lot of batteries. For the purpose of comparison, the conduction losses of diode are estimated for both the proposed equalizer and the general equalizer. Fig. 14(b) shows the estimated conduction loss of a diode as a percentage of the total losses, and the percentages of a diode loss over total loss decrease for the proposed equalizer. From the experiments, the measured maximum efficiency for the proposed charge equalizer is up to 91.2%, and the measured efficiencies are close to the estimated values as shown in Fig. 14(c).

Although the state-of-charge balancing can efficiently distribute the energy among the batteries since it can deliver the

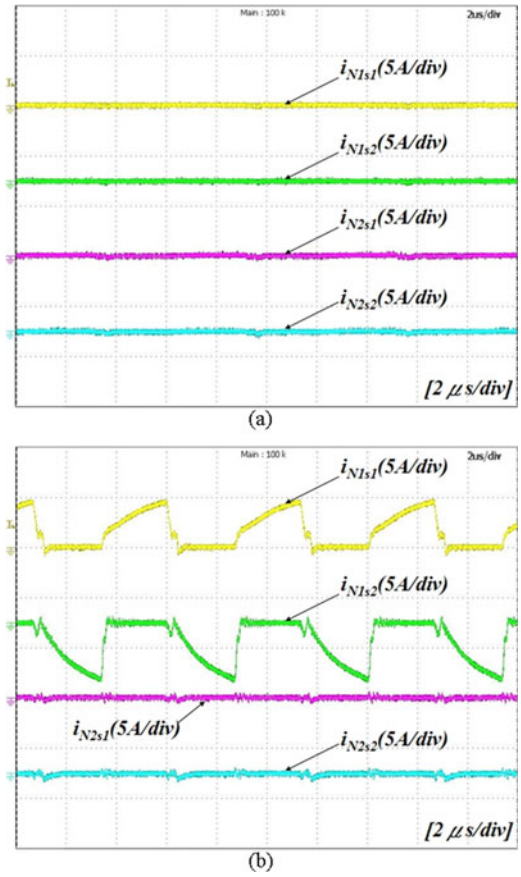

Fig. 12. Measured secondary-side currents of the transformer. (a) All battery module voltages are the same. (b) Battery module M_1 has the lowest voltage in the battery pack.

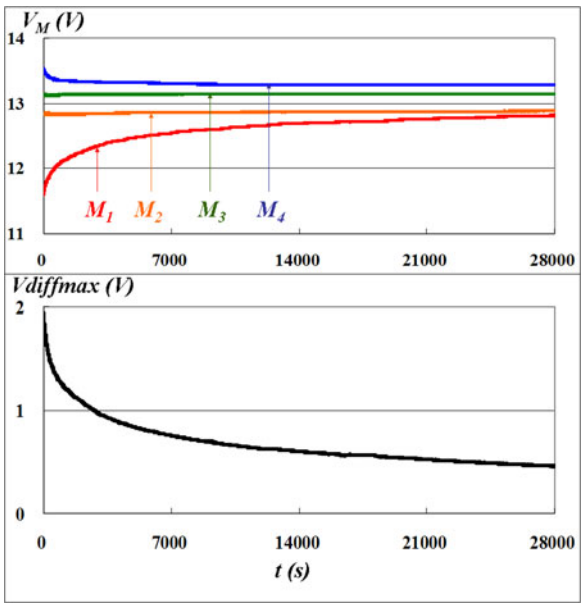

Fig. 13. Charge equalization result.

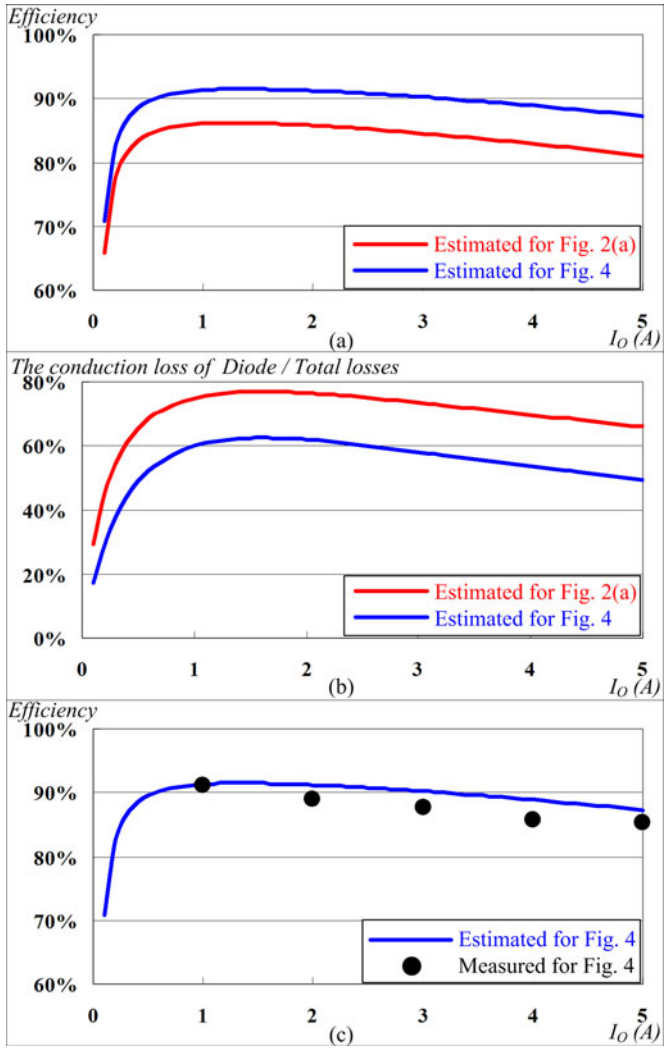

Fig. 14. Efficiency analysis. (a) Estimated efficiencies. (b) Estimated conduction loss of the diode as a percentage of the total losses. (c) Estimated and measured efficiencies for the proposed charge equalizer.

energy from a low-voltage battery to a high-voltage battery, a complex control and more active switches are required. To simplify the control strategy and the circuit structure in this paper, the voltage balancing principle is applied for the proposed charge equalizer due to its easy implementation. On the other hand, the proposed charge equalizer is simple since it uses only two active switches, and the circuit at secondary side can be easily expanded for the system with a lot of batteries. Moreover, the maximum flux density of the transformer core has to be considered based on Faraday's law, and the voltage rating of each active switch has to be higher than the voltage of battery pack for the system. In short, the proposed charge equalizer has very good scalability for the battery system with a lot of batteries.

VI. Conclusion

In the EV applications, the performance of charge equalizer is a key factor which directly affects the reliability of a battery system. Therefore, a charge equalizer with fewer active components

is preferred for the reliability of the battery system. This paper has presented a charge equalizer with a combination of APWM and PFM control based on a modified half-bridge converter. The split capacitors are not used and the soft switching of power switches can be achieved, which enhance the reliability of the charge equalizer. In addition, the battery charge equalization can be flexibly controlled by a PFM control. A new rectification is designed for the charge equalizer; thus, the number of the bridge rectifiers at the secondary side of transformer can be reduced by half. The system cost and the conduction loss are also cut by half. To simplify the layout of PCB, four rectifier diodes can be replaced by one bridge rectifier. Finally, the experimental results are provided to verify the feasibility and performance of the proposed charge equalizer.

REFERENCES

[1] A. Manenti, A. Abba, A. Merati, S. M. Savaresi, and A. Geraci, "A new BMS architecture based on cell redundancy," *IEEE Trans. Ind. Electron.*, vol. 58, no. 9, pp. 4314–4321, Sep. 2011.

[2] M.-Y. Kim, C.-H. Kim, J.-H. Kim, and G.-W. Moon, "A chain structure of switched capacitor for improved cell balancing speed of lithium-ion batteries," *IEEE Trans. Ind. Electron.*, vol. 61, no. 8, pp. 3989–3999, Aug. 2014.

[3] M. Uno and K. Tanaka, "Influence of high-frequency charge–discharge cycling induced by cell voltage equalizers on the life performance of lithium-ion cells," *IEEE Trans. Veh. Technol.*, vol. 60, no. 4, pp. 1505–1515, May 2011.

[4] H.-S. Park, C.-H. Kim, K.-B. Park, G.-W. Moon, and J.-H. Lee, "Design of a charge equalizer based on battery modularization," *IEEE Trans. Veh. Technol.*, vol. 58, no. 7, pp. 3216–3223, Sep. 2009.

[5] F. Baronti, C. Bernardeschi, L. Cassano, A. Domenici, R. Roncella, and R. Saletti, "Design and safety verification of a distributed charge equalizer for modular Li-ion batteries," *IEEE Trans. Ind. Informat.*, vol. 10, no. 2, pp. 1003–1011, May 2014.

[6] C.-H. Kim, M.-Y. Kim, and G.-W. Moon, "A modularized charge equalizer using a battery monitoring IC for series-connected Li-ion battery strings in electric vehicles," *IEEE Trans. Power Electron.*, vol. 28, no. 8, pp. 3779–3787, Aug. 2013.

[7] C.-S. Lim, K.-J. Lee, N.-J. Ku, D.-S. Hyun, and R.-Y. Kim, "A modularized equalization method based on magnetizing energy for a series-connected lithium-ion battery string," *IEEE Trans. Power Electron.*, vol. 29, no. 4, pp. 1791–1799, Apr. 2014.

[8] F. Baronti, G. Fantechi, R. Roncella, and R. Saletti, "High-efficiency digitally controlled charge equalizer for series-connected cells based on switching converter and super-capacitor," *IEEE Trans. Ind. Informat.*, vol. 9, no. 2, pp. 1139–1147, May 2013.

[9] J. Kim, J. Shin, C. Chun, and B.-H. Cho, "Stable configuration of a Li-ion series battery pack based on a screening process for improved voltage/soc balancing," *IEEE Trans. Power Electron.*, vol. 27, no. 1, pp. 411–424, Jan. 2012.

[10] P. A. Cassani and S. S. Williamson, "Design, testing, and validation of a simplified control scheme for a novel plug-in hybrid electric vehicle battery cell equalizer," *IEEE Trans. Ind. Electron.*, vol. 57, no. 12, pp. 3956–3962, Dec. 2010.

[11] J. D. Dogger, B. Roossien, and F. D. J. Nieuwenhout, "Characterization of Li-ion batteries for intelligent management of distributed grid-connected storage," *IEEE Trans. Energy Convers.*, vol. 26, no. 1, pp. 256–263, Mar. 2011.

[12] M. A. Roscher, J. Assfalg, and O. S. Bohlen, "Detection of utilizable capacity deterioration in battery systems," *IEEE Trans. Veh. Technol.*, vol. 60, no. 1, pp. 98–103, Jan. 2011.

[13] P. A. Cassani and S. S. Williamson, "Feasibility analysis of a novel cell equalizer topology for plug-in hybrid electric vehicle energy-storage systems," *IEEE Trans. Veh. Technol.*, vol. 58, no. 8, pp. 3938–3946, Oct. 2009.

[14] L. Lam and P. Bauer, "Practical capacity fading model for Li-ion battery cells in electric vehicles," *IEEE Trans. Power Electron.*, vol. 28, no. 12, pp. 5910–5918, Dec. 2013.

[15] H. A.-H. Hussein and I. Batarseh, "A review of charging algorithms for nickel and lithium battery chargers," *IEEE Trans. Veh. Technol.*, vol. 60, no. 3, pp. 830–838, Mar. 2011.

[16] S.-H. Park, K.-B. Park, H.-S. Kim, G.-W. Moon, and M.-J. Youn, "Single-magnetic cell-to-cell charge equalization converter with reduced number of transformer windings," *IEEE Trans. Power Electron.*, vol. 27, no. 6, pp. 2900–2911, Jun. 2012.

[17] Y.-H. Hsieh, T.-J. Liang, S.-M. Chen, W.-Y. Horng, and Y.-Y. Chung, "A novel high-efficiency compact-size low-cost balancing method for series-connected battery applications," *IEEE Trans. Power Electron.*, vol. 28, no. 12, pp. 5927–5939, Dec. 2013.

[18] H.-S. Park, C.-E. Kim, C.-H. Kim, G.-W. Moon, and J.-H. Lee, "A modularized charge equalizer for an HEV lithium-ion battery string," *IEEE Trans. Ind. Electron.*, vol. 56, no. 5, pp. 1464–1476, May 2009.

[19] M. Einhorn, W. Roessler, and J. Fleig, "Improved performance of serially connected Li-ion batteries with active cell balancing in electric vehicles," *IEEE Trans. Veh. Technol.*, vol. 60, no. 6, pp. 2448–2457, Jul. 2011.

[20] T. H. Phung, A. Collet, and J.-C. Crebier, "An optimized topology for next-to-next balancing of series-connected lithium-ion cells," *IEEE Trans. Power Electron.*, vol. 29, no. 9, pp. 4603–4613, Sep. 2014.

[21] M. Uno and K. Tanaka, "Single-switch cell voltage equalizer using multistacked buck-boost converters operating in discontinuous conduction mode for series-connected energy storage cells," *IEEE Trans. Veh. Technol.*, vol. 60, no. 8, pp. 3635–3645, Oct. 2011.

[22] A. C. Baughman and M. Ferdowsi, "Double-tiered switched-capacitor battery charge equalization technique," *IEEE Trans. Ind. Electron.*, vol. 55, no. 6, pp. 2277–2285, Jun. 2008.

[23] M.-Y. Kim, J.-H. Kim, and G.-W. Moon, "Center-cell concentration structure of a cell-to-cell balancing circuit with a reduced number of switches," *IEEE Trans. Power Electron.*, vol. 29, no. 10, pp. 5285–5297, Oct. 2014.

[24] Y. Yuanmao, K. W. E. Cheng, and Y. P. B. Yeung, "Zero-current switching switched-capacitor zero-voltage-gap automatic equalization system for series battery string," *IEEE Trans. Power Electron.*, vol. 27, no. 7, pp. 3234–3242, Jul. 2012.

[25] J. Ewanchuk and J. Salmon, "A modular balancing bridge for series connected voltage sources," *IEEE Trans. Power Electron.*, vol. 29, no. 9, pp. 4712–4722, Sep. 2014.

[26] F. Mestrallet, L. Kerachev, J.-C. Crebier, and A. Collet, "Multiphase interleaved converter for lithium battery active balancing," *IEEE Trans. Power Electron.*, vol. 29, no. 6, pp. 2874–2881, Jun. 2014.

[27] A. Xu, S. Xie, and X. Liu, "Dynamic voltage equalization for series-connected ultracapacitors in EV/HEV applications," *IEEE Trans. Veh. Technol.*, vol. 58, no. 8, pp. 3981–3987, Oct. 2009.

[28] M. Vasiladiotis and A. Rufer, "Analysis and control of modular multilevel converters with integrated battery energy storage," *IEEE Trans. Power Electron.*, vol. 30, no. 1, pp. 163–175, Jan. 2015.

[29] W. Wang, H. S.-H. Chung, and J. Zhang, "Near-real-time parameter estimation of an electrical battery model with mulitple time consonants and SOC-dependent capacitance," *IEEE Trans. Power Electron.*, vol. 29, no. 11, pp. 5905–5920, Nov. 2014.

Chihchiang Hua (S'91–M'92) received the B.S. degree in electrical engineering from National Cheng Kung University, Tainan, Taiwan, in 1984, and the M.S. and Ph.D. degrees in electrical engineering from the University of Missouri, Columbia, MO, USA, in 1990 and 1992, respectively.

Since 1992, he has been with the National Yunlin University of Science and Technology, Douliou, Taiwan, where he is currently a Professor at the Department of Electrical Engineering. His research interests include power electronics converters, uninterruptible power supplies, and photovoltaic/wind energy systems.

Dr. Hua is a Member of the IEEE Power Electronics and the IEEE Industrial Electronics Societies.

Yi-Hsiung Fang received the B.S. and M.S. degrees in electrical engineering from the National Yunlin University of Science and Technology, Douliou, Yunlin, Taiwan, in 2011 and 2013, respectively, where he is currently working toward the Ph.D. degree at the Graduate School of Engineering Science and Technology.

His research interests include the design and implementation of battery chargers, battery charge equalizers, and high-efficiency power converters.